



Numerical Investigation on Dissociation Performance of Natural Gas Hydrate in Reservoirs by Depressurization

Lin Dong^(✉) and Hualin Liao

School of Petroleum Engineering, China University of Petroleum (East China),
Qingdao 266580, China
donglinupc@163.com

Abstract. The velocity of dissociation front is key factor to reflect the hydrate production process. However, the characteristics of dissociation front and formation responses during hydrate production are not studied in detail. To investigate the dissociation performance of gas hydrate, we conduct a numerical model to simulate the process of gas extraction from formation by depressurization. The distribution of hydrate, water, and gas saturation varies during production process. The hydrate saturation decreases in near-well region, while the gas saturation increases. The dissociation zone expands and dissociation front moves from well to formation. This work can provide a reference for natural gas development.

Keywords: Natural gas hydrate · Dissociation performance · Front movement · Gas extraction · Physical fields

Symbol Description

P_i	Initial pore pressure
T_i	Initial temperature
S_h, S_w	Hydrate and water saturation
P_f	Well pressure
T_f	Well temperature
$\lambda_h, \lambda_w, \lambda_g, \lambda_s$	Thermal conductivity of hydrate, water, gas, and sand
C_s, C_w, C_g, C_r, C_h	Specific heat of sediments, water, gas, rock, and hydrate
ρ_r, ρ_h, ρ_d	Density of rock, hydrate, and drilling fluid
K_0	Initial permeability (hydrate-free)
ΔE_a	Activation energy
M_{H_2O}, M_{CH_4}, M_h	Molar mass of water, methane, and hydrate
r_w	Borehole radius
φ	Porosity
k_{d0}	Intrinsic kinetic constant
N_h	Hydration number
S_{wr}, S_{gr}	Irreducible water and gas saturation
P_0	Gas entry value

1 Introduction

Natural gas hydrate (NGH) is one of the most important sources of alternative energy, which draws the attention to the whole world [1, 2]. Generally, NGH widely exists in oceanic and permafrost regions under the condition of high pressure and low temperature [3]. Driven by the energy demand and technological advancement, natural gas hydrate production is conducted worldwide to extract natural gas from the reservoirs, such as the South China Sea and the Eastern Nankai Trough [4, 6].

Changes in physical fields and dissociation front are important for analyzing production performance during gas extraction from natural gas hydrate reservoirs [6]. Zheng et al. [7] studied the controlling mechanisms of hydrate dissociation front with the lab-scale and field-scale models. The results indicate that using optimized characteristic time is a key factor in establishing calculation models. Afterward, A pragmatic criterion was developed to illustrate the relations among controlling mechanisms, hydrate dissociation modes, and characteristics of dissociation front [8]. Besides, the investigation on advance of dissociation front is essential for optimizing gas production and preventing the risks [9]. However, the dissociations on characteristics of dissociation front and formation responses during hydrate production are insufficient.

In this paper, we investigate the dissociation performance of gas hydrate reservoirs by depressurization method. The responses of pore pressure and temperature of formation are discussed. Besides, the distribution of hydrate, water, and gas saturation as well as dissociation front of hydrate are studied. This work can provide a reference for the practical application and numerical simulation in natural gas hydrate development.

2 Numerical Model

2.1 Governing Equations

The continuity equation of hydrate, water, and gas are given as follows:

$$\frac{\partial(\varphi\rho_h S_h)}{\partial t} = -m_h \quad (1)$$

$$\frac{\partial(\varphi\rho_w S_w)}{\partial t} - \nabla \cdot \left[\frac{K_{rw} K \rho_w}{\mu_w} (p_w + \rho_w g) \right] = m_w \quad (2)$$

$$\frac{\partial(\varphi\rho_g S_g)}{\partial t} - \nabla \cdot \left[\frac{K_{rg} K \rho_g}{\mu_g} (p_g + \rho_g g) \right] = m_g \quad (3)$$

The dissociation process of hydrate in the reservoirs can be described by the Kim-Bishoni kinetic model.

$$m_g = k_{d0} \exp\left(\frac{\Delta E_a}{RT}\right) M_{CH_4} A_{rs} (p_e - p_g) \quad (4)$$

$$A_{rs} = \varphi S_h \sqrt{\frac{\varphi(1 - S_h)}{2K}} \quad (5)$$

$$K = K_0(1 - S_h)^n \quad (6)$$

Correspondingly, the generation rate of water and dissociation rate of hydrate are showed as follows:

$$m_w = m_g N_h \frac{M_{H_2O}}{M_{CH_4}} \quad (7)$$

$$m_h = -m_g \frac{M_H}{M_{CH_4}} \quad (8)$$

$$P_e = \exp\left(A_0 + A_1 T + A_2 T^2 + A_3 T^3 + A_4 T^4 + A_5 T^5\right) \quad (9)$$

$$p_w = p_g - p_c \quad (10)$$

The energy conservation is expressed as:

$$\frac{\partial [\rho_w \varphi S_w C_w T + \rho_g \varphi S_g C_g T + \rho_h \varphi S_h C_h T + \rho_s (1 - \varphi) C_s T]}{\partial t} + \quad (11)$$

$$\nabla \cdot (\rho_w \varphi S_w \mathbf{v}_{w,i} C_w T + \rho_g \varphi S_g \mathbf{v}_{g,i} C_g T) = \nabla \cdot \lambda_{eff} \nabla T + Q_h$$

$$Q_h = \frac{m_h}{M_h} (B_1 + B_2 T) \quad (12)$$

The heat transfer coefficient of the HBS can be determined by the sediments, hydrate, water, and gas.

$$\lambda_{eff} = (1 - \varphi) \lambda_s + \varphi (S_g \lambda_g + S_w \lambda_w + S_h \lambda_h) \quad (13)$$

Capillary pressure is given based on Van-Genuchten model.

$$p_c = p_0 \left[\left(\frac{S_w - S_{wr}}{1 - S_{wr}} \right)^{-1/\lambda} - 1 \right]^{1-\lambda} \quad (14)$$

The relative permeability of water and gas endpoints of hydrate-free sediments are calculated by the following equations.

$$K_{rw} = K_{rwo} \left(\frac{S_w - S_{wr}}{1 - S_{wr}} \right)^{n_w} \quad (15)$$

$$K_{rg} = K_{rgo} \left(\frac{S_g - S_{gr}}{1 - S_{gr}} \right)^{n_g} \quad (16)$$

2.2 Model Descriptions

Figure 1 shows the cylindrical model of natural gas hydrate reservoir. The radius is 100 m and the height is set as 20 m. A well is designed in the centre of this model which is used for producing natural gas from this reservoir.

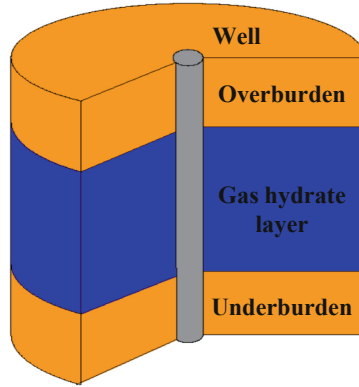


Fig.1. Model construction for the simulation.

2.3 Initial and Boundary Conditions

The initial conditions in this model are determined by referring the previous studies [10]. The initial formation temperature and pore pressure are set as 288.15K and 14MPa, respectively. Besides, the initial water and hydrate saturation are 0.5 and 0.5, respectively.

The parameters are determined according to the previous studies and geological data in the South China Sea [11, 12], as shown in Table 1.

Table 1. Parameters used in this model.

Parameter	Value
Initial pore pressure, P_i	14 MPa
Initial temperature, T_i	288.15 K
Hydrate saturation, S_h	0.5
Water saturation, S_w	0.5
Well pressure, P_f	4.0 MPa
Well temperature, T_f	278.15K
Thermal conductivity of hydrate, λ_h	$2.0 \text{ W}\cdot\text{m}^{-1}\cdot\text{K}^{-1}$
Thermal conductivity of water, λ_w	$0.6 \text{ W}\cdot\text{m}^{-1}\cdot\text{K}^{-1}$
Thermal conductivity of gas, λ_g	$0.07 \text{ W}\cdot\text{m}^{-1}\cdot\text{K}^{-1}$
Thermal conductivity of sand, λ_s	$1.0 \text{ W}\cdot\text{m}^{-1}\cdot\text{K}^{-1}$
Specific heat of sediments, C_s	$1000 \text{ J}\cdot\text{kg}^{-1}\cdot\text{K}^{-1}$
Specific heat of water, C_w	$4200 \text{ J}\cdot\text{kg}^{-1}\cdot\text{K}^{-1}$
Specific heat of gas, C_g	$2180 \text{ J}\cdot\text{kg}^{-1}\cdot\text{K}^{-1}$

(continued)

Table 1. (continued)

Parameter	Value
Specific heat of hydrate, C_h	2220 J·kg ⁻¹ ·K ⁻¹
Density of rock, ρ_r	2600kg/m ³
Density of hydrate, ρ_h	920kg/m ³
Density of drill fluid, ρ_f	1019kg/m ³
Initial permeability (hydrate-free), K_0	10 mD
Activation energy, ΔE_a	81084.20J·mol ⁻¹
Molar mass of water, M_{H2O}	18.016g·mol ⁻¹
Molar mass of methane gas, M_{CH4}	16.042g·mol ⁻¹
Molar mass of methane hydrate, M_h	124.138g·mol ⁻¹
Borehole radius, r_w	0.15 m
Porosity, φ	0.40
Intrinsic kinetic constant, k_{d0}	3.6 × 10 ⁴ mol·m ⁻² ·Pa ⁻¹ ·s ⁻¹
Hydration number, N_h	6
Irreducible water saturation, S_w	0.3
Irreducible water saturation, S_{gr}	0.05
λ	0.7
Gas entry value, P_0	10 ⁵ Pa
C_f	33.72995
C_1	13521
C_2	-4.02

3 Results and Discussions

3.1 Description of Specimens

Figure 2 shows the distribution of pore pressure during gas hydrate production. The pore pressure increases from near-well region to far well formation. The depressurization and hydrate dissociation lead to the changes in the pore pressure field, which reflects the mass transfer process with the multi-phase flow.

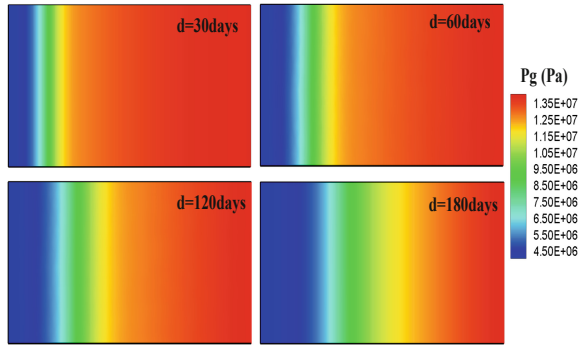


Fig. 2. Variation of pore pressure versus production time

Figure 3 illustrates the distribution of temperature in the natural gas hydrate formation. The temperature increases from well to formation, which is caused by the heat transfer and hydrate dissociation. The distribution of temperature varies during production process due to the heat and mass transfer.

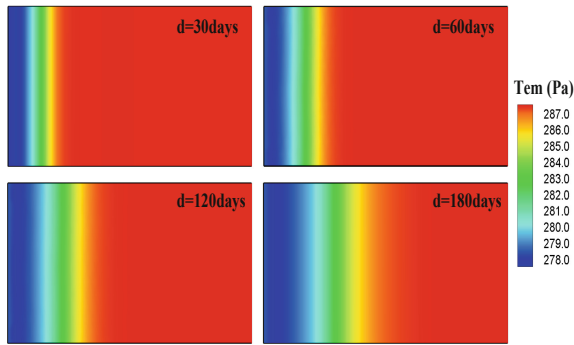


Fig. 3. Variation of the temperature of formation versus production time

3.2 Variation of Hydrate, Gas, and Water Saturation

Distribution of hydrate and water saturation during gas hydrate production are displayed in Figs. 4 and 5. The results indicate that the hydrate saturation decreases significantly with production time. Meanwhile, it is lower near well induced by the hydrate dissociation compared with that in the zone far from the well.

In addition, the water saturation increases due to the produced water from the hydrate dissociation. The water in the formation is also extracted to the ground. These factors affect the water distribution in the formation. The phase transition of hydrate occurs during production, which brings in variation of hydrate and water saturation.

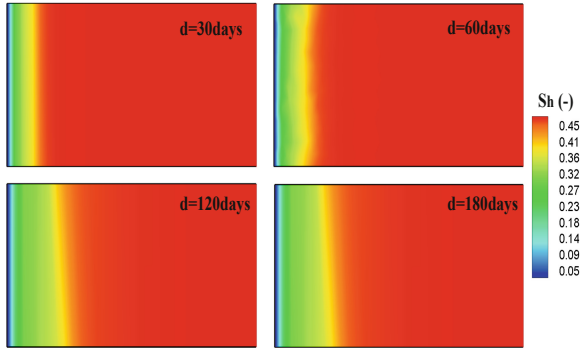


Fig. 4. Distribution of hydrate saturation during hydrate production

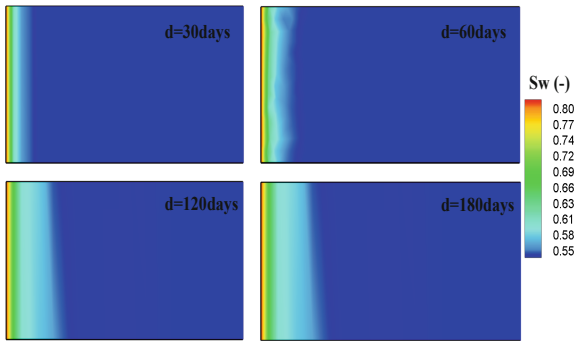


Fig. 5. Distribution of water saturation during hydrate production

Similarly, the gas saturation increases in near well region, which is caused by the hydrate dissociation and gas extraction, as shown in Fig. 6. The gas produced through hydrate dissociation is extracted from the formation, which leads to the variation of gas saturation and changes in distribution characteristics.

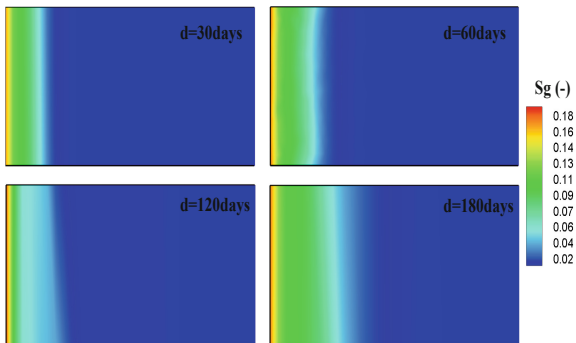


Fig. 6. Distribution of gas saturation during hydrate production

3.3 Hydrate Dissociation Front

Figure 7 demonstrates the variation of hydrate saturation during gas extraction. It can be observed that the hydrate saturation in near-well region is lower. The dissociation zone expands with production time, as shown in Fig. 7(b). The hydrate dissociation front moves toward the further bore zone due to the changes in the dissociation zone.

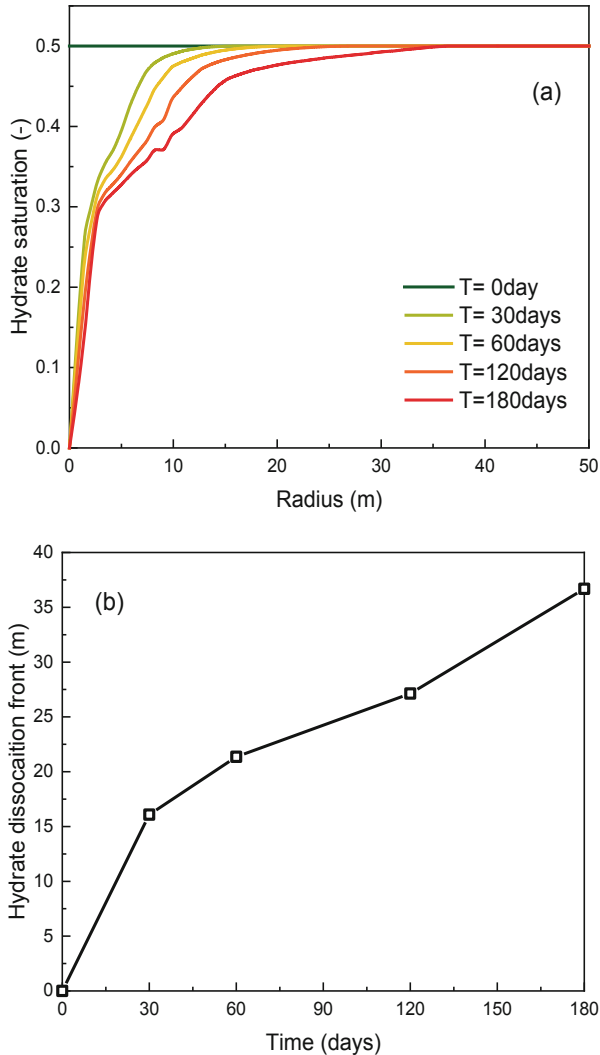


Fig. 7. Variation of hydrate saturation and dissociation front during production

As mentioned above, the controlling mechanisms of hydrate dissociation and characteristics of dissociation front depend on the pressure and temperature conditions of the

well and the properties of the formation. The dissociation front reflects the production process of the natural gas hydrate.

4 Conclusion

Based on the results and discussions presented above, the conclusions are obtained as below:

- (1) Dissociation performance of natural gas hydrate in the formation is a complex process associated with heat and mass transfer as well as phase transition. Numerical simulation on hydrate production provides the references of dissociation characteristics and changes in physical fields for analyzing natural gas hydrate production.
- (2) Distribution of multi-physical fields varies during hydrate dissociation, which is determined by the gas extraction as well as the heat and mass transfer process. The hydrate saturation decreases in near-well formation, while the gas saturation increases.
- (3) The dissociation zone expands, and hydrate dissociation front moves to far well formation with production time. The multi-field responses of natural gas hydrate reservoirs are related to the hydrate dissociation performance during natural gas hydrate production.

Acknowledgments. This research was supported by , Graduate School Innovation Program of China University of Petroleum (YCX2019020). These financial supports are gratefully acknowledged. We recognize the support of China University of Petroleum (East China) for the permission to publish this paper.

References

1. Boswell, R., Collett, T.S.: Current perspectives on gas hydrate resources. *Energy Environ. Sci.* **4**(4), 1206–1215 (2011)
2. Chong, Z.R., Yang, S.H.B., Babu, P., Linga, P., Li, X.: Review of natural gas hydrates as an energy resource: prospects and challenges. *Appl. Energy* **162**, 1633–1652 (2016)
3. Waite, W.F., et al.: Physical properties of hydrate-bearing sediments. *Rev. Geophys.* **47**(4), 1–38 (2009)
4. Malagar, B.R.C., Lijith, K.P., Singh, D.N.: Formation & dissociation of methane gas hydrates in sediments: a critical review. *J. Nat. Gas Sci. Eng.* **65**, 168–184 (2019)
5. Qin, X., et al.: The response of temperature and pressure of hydrate reservoirs in the first gas hydrate production test in South China Sea. *Appl. Energy* **278**, 115649 (2020)
6. Yu, T., Guan, G., Abudula, A., Yoshida, A., Wang, D., Song, Y.: Gas recovery enhancement from methane hydrate reservoir in the Nankai Trough using vertical wells. *Energy (Oxford)* **166**, 834–844 (2019)
7. Zheng, R., Li, S., Cui, G.: Determining the controlling mechanisms of hydrate dissociation front using optimized characteristic time. *Fuel* **298**, 120805 (2021)

8. Zheng, R., Li, S., Li, Q., Li, X.: Study on the relations between controlling mechanisms and dissociation front of gas hydrate reservoirs. *Appl. Energy* **215**, 405–415 (2018)
9. Bhade, P., Phirani, J.: Gas production from layered methane hydrate reservoirs. *Energy* **2**, 686–696 (2015)
10. Feng, Y., et al.: Numerical analysis of gas production from layered methane hydrate reservoirs by depressurization. *Energy* **166**, 1106–1119 (2019)
11. Sun, X., Luo, T., Wang, L., Wang, H., Song, Y., Li, Y.: Numerical simulation of gas recovery from a low-permeability hydrate reservoir by depressurization. *Appl. Energy* **250**, 7–18 (2019)
12. Wan, Y., et al.: Reservoir stability in the process of natural gas hydrate production by depressurization in the shenhu area of the south China sea. *Nat. Gas Indus. B* **5**(6), 631–643 (2018)